CHINESE OPTICS LETTERS

Vol. 22, No. 4 | April 2024

Erbium-ytterbium co-doped lithium niobate single-mode microdisk laser with an ultralow threshold of 1 μW

Minghui Li (李明慧)[1,2], Renhong Gao (高仁宏)[1,2], Chuntao Li (黎春桃)[3,4], Jianglin Guan (管江林)[3,4], Haisu Zhang (张海粟)[3], Jintian Lin (林锦添)[1,2*], Guanghui Zhao (赵光辉)[1,5], Qian Qiao (乔 迁)[1,5], Min Wang (汪 旻)[2], Lingling Qiao (乔玲玲)[1], Li Deng (邓 莉)[2], and Ya Cheng (程 亚)[1,2,3,6,7**]

[1] State Key Laboratory of High Field Laser Physics and CAS Center for Excellence in Ultra-Intense Laser Science, Shanghai Institute of Optics and Fine Mechanics (SIOM), Chinese Academy of Sciences (CAS), Shanghai 201800, China

[2] Center of Materials Science and Optoelectronics Engineering, University of Chinese Academy of Sciences, Beijing 100049, China

[3] XXL—The Extreme Optoelectromechanics Laboratory, School of Physics and Electronic Science, East China Normal University, Shanghai 200241, China

[4] State Key Laboratory of Precision Spectroscopy, East China Normal University, Shanghai 200062, China

[5] School of Physical Science and Technology, ShanghaiTech University, Shanghai 200031, China

[6] Shanghai Research Center for Quantum Sciences, Shanghai 201315, China

[7] Hefei National Laboratory, Hefei 230088, China

*Corresponding author: jintianlin@siom.ac.cn

**Corresponding author: ya.cheng@siom.ac.cn

Received September 19, 2023 | Accepted December 15, 2023 | Posted Online April 17, 2024

We demonstrate single-mode microdisk lasers in the telecom band with ultralow thresholds on erbium-ytterbium co-doped thin-film lithium niobate (TFLN). The active microdisk was fabricated with high-*Q* factors by photolithography-assisted chemomechanical etching. Thanks to the erbium-ytterbium co-doping providing high optical gain, the ultralow loss nanostructuring, and the excitation of high-*Q* coherent polygon modes, which suppresses multimode lasing and allows high spatial mode overlap between pump and lasing modes, single-mode laser emission operating at 1530 nm wavelength was observed with an ultralow threshold, under a 980-nm-band optical pump. The threshold was measured as low as 1 μW, which is one order of magnitude smaller than the best results previously reported in single-mode active TFLN microlasers. The conversion efficiency reaches 4.06×10^{-3}, which is also the highest value reported in single-mode active TFLN microlasers.

Keywords: lithium niobate; microcavities; microdisk lasers.
DOI: 10.3788/COL202422.041301

1. Introduction

An intense desire for high-performance photonic integrated devices such as electro-optic modulators[1–3], optical frequency conversion[4–11], quantum light sources[12–15], optical frequency combs[16–22], and ultrafast pulse generation[23], rapidly motivates the photonic integration platforms to lithium-niobate-on-insulator (LNOI) wafer[24–27], owing to the outstanding material properties of lithium niobate, such as a broad transparency window (350 nm to 5 μm), a large linear electro-optic, second-order nonlinear, acoustic-optic, and piezo-electric coefficients[24–28]. All the above-mentioned applications have been successfully demonstrated on passive LNOI wafers with unparalleled performance due to the accessible highly confined photonic structures with ultralow loss due to the rapid developments in ion-slicing technique and LNOI nanofabrication technology. The development of scalable photonic integrated circuits also raises the interest in doping rare-earth ions into LNOI photonic structures to add functionalities enabled by the active ions, for example, microlasers[29–34], optical waveguide amplifiers[35–37], and quantum photonic devices[38]. Among these devices, single-mode microlasers have been demonstrated in erbium ion-doped microcavities[29–34,39–41], serving as coherent light sources operating in the telecom waveband. A threshold as low as 25 μW has been reported[30,42], and the highest conversion efficiency reached 1.8×10^{-3}[33]. However, there is still plenty of room for improvement in the conversion efficiency and threshold of single-mode microlasers.

To improve the optical gain of erbium ions, ytterbium ions have been often used as sensitizers to enhance the excitation rates as well as to reduce the concentration quenching of erbium ions via resonant energy transfer, facilitating an improved pumping efficiency in the 980-nm band[43,44]. Due to the

difficulty in the growth of the co-doped lithium niobate crystal and the fabrication of co-doped thin-film LNOI, erbium and ytterbium ions have only recently been co-doped in LNOI devices, leading to multimode microlasers of low threshold[45] and optical waveguide amplifiers with a net small-signal gain as high as 27 dB[46]. However, because there are a large number of whispering gallery modes (WGMs) within optical gain bandwidth, single-mode microlasers have not been reported on the co-doped LNOI platform.

In this work, single-mode microlasers are demonstrated in an erbium, ytterbium co-doped LNOI microdisk with a diameter of 40 μm. Weak perturbation was introduced into the circular microdisk to organize the traditional WGMs as polygon modes[30,47]. When the polygon mode in the weakly perturbed microdisk was excited around 980 nm wavelength, a single-mode lasing signal was observed at 1530 nm wavelength, benefiting from the significant suppression of the large number of WGMs within the gain bandwidth. A laser threshold as low as 1 μW was measured, which is enabled by the high optical gain of co-doping and the excitation of a high-Q polygon mode. The conversion efficiency reaches 4.06×10^{-3}. Both these values are the state-of-the-art results in single-mode active LNOI microlasers in the telecom band[42].

2. Fabrication Methods

The fabrication of erbium-ytterbium co-doped Z-cut LNOI microdisks begins from the growth of the co-doped lithium niobate bulk crystal using the Czochralski method. The doping concentrations of 0.1% (erbium) and 0.1% (ytterbium) were adopted to provide high optical gain. Then ion implantation, silica deposition, bonding, chemomechanical polishing (CMP), and annealing were carried out to produce the co-doped thin-film LNOI wafer. The LNOI wafer consists of a 500-nm-thick co-doped lithium niobate thin film, a 2-μm-thick silica layer, and a 500-μm-thick silicon handle. The microdisks were fabricated on the co-doped LNOI wafer by the home-built photolithography-assisted chemomechanical polishing (PLACE) technique[48]. To fabricate the microdisk by PLACE, first, a chromium (Cr) layer with a thickness of 200 nm was deposited on the surface of LNOI by the magnetron sputtering method. Subsequently, a microdisk-shaped pattern was produced in the Cr layer using spatial selective femtosecond laser ablation with a resolution of ~200 nm, which serves as a hard mask in the next etching step. Next, the CMP process was conducted to etch the exposed lithium niobate underneath the Cr mask. Therefore, the pattern was transferred from the Cr layer to the thin-film lithium niobate layer. Third, the sample was immersed in a Cr etching solution for 20 min to remove the Cr layer. Fourth, a secondary CMP process was carried out to improve the smoothness of the fabricated LNOI microdisk. Finally, the silica underneath the lithium niobate microdisk was partially undercut by chemical wet etching. The scanning electron microscopy (SEM) images of the fabricated microdisk are shown in Fig. 1, where the diameter of the microdisk was ~44 μm.

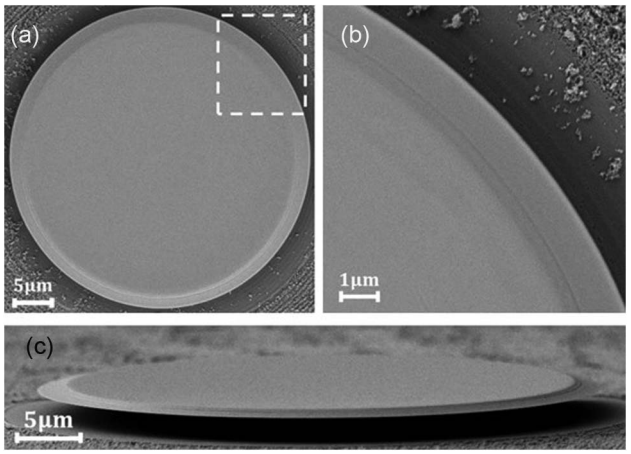

Fig. 1. SEM images of the microdisk. (a) Top view; (b) enlarged SEM image of the microdisk indicated by a rectangle in (a), showing a smooth sidewall; (c) oblique view.

3. Experimental Setup for the Microlaser and Q-factor Measurement

To demonstrate a single-mode microlaser from polygon modes, the Q factors of the pump mode and lasing mode were characterized. The experimental setup for Q-factor measurement and lasing is illustrated in Fig. 2(a). A tunable laser (TLB-6719, New Focus Inc.) with linewidth < 200 kHz connected with an inline

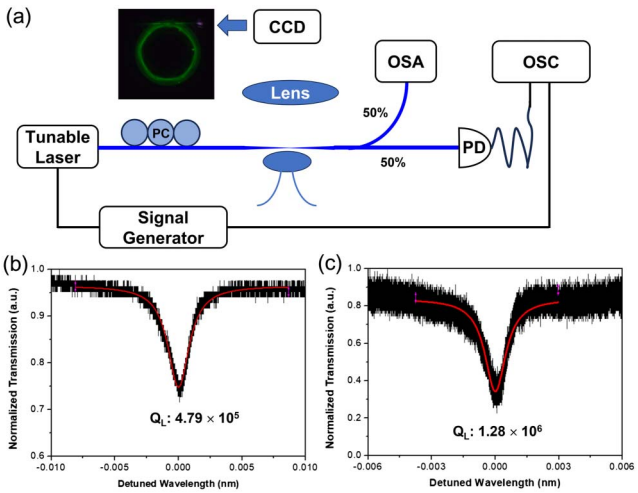

Fig. 2. (a) Schematic of experimental setup. Inset, the optical microscope image of the upconversion fluorescence distributed in the microdisk, exhibiting a hexagon pattern. OSA, optical spectrum analyzer; PD, photodetector; PC, polarization controller; CCD, charge-coupled device; OSC, oscilloscope. (b) Lorentz fitting (red curve) of the pump mode around 974.79 nm, revealing a loaded Q factor of 4.79×10^5; (c) Lorentz fitting (red curve) of the lasing mode around 1531.40 nm, exhibiting a loaded Q factor of 1.28×10^6.

polarization controller (PC) was used as the pump light, allowing a large wavelength scanning range from 940 to 985 nm. The pump light was coupled into the microdisk through a tapered fiber with a waist of 2.0 μm. The tapered fiber was placed in close contact with the top surface of the circular microdisk at the position that was ~18.5 μm far from the disk center to introduce weak perturbation for the formation of polygon modes resonant with both the lasing and pump wavelengths. The coupled position was controlled by a 3D piezo-electric stage with a resolution of 20 nm. A microscope imaging system consisting of an objective lens with numerical aperture of 0.28 and a charge-coupled device was mounted above the weakly perturbed microdisk to monitor and capture the optical field distribution in the microdisk. The generated signal was coupled out of the microdisk by the same tapered fiber, and separately sent to an optical spectrum analyzer (OSA, AQ6370D, Yokogawa Inc.) and a photodetector (1611-FC, New Focus Inc.) connected with an oscilloscope (MDO3104, Tektronix Inc.) for optical spectrum analysis and transmission spectrum measurement, respectively. To measure the Q factor of the pump polygon mode, a ramp signal was sent to the tunable laser for fine wavelength scanning across the resonant wavelength. A weak input power as low as 0.5 μW was chosen to avoid the thermal-optic effect and lasing. And the transmission spectrum of the tapered fiber was recorded by the oscillation during wavelength scanning. To measure the Q factor of the lasing polygon mode, another tunable laser (TLB-6728, New Focus Inc.) replaced the above-mentioned laser, working in the telecom band. Once the pump wavelength was adjusted to resonant with the polygon pump mode with above-threshold pump power, lasing signals were detected and recorded by the OSA.

Sharp dips will appear in the transmission spectrum when the scanning wavelength is resonant with the modes. The Q factors of the pump and lasing polygon modes are plotted in Figs. 2(b) and 2(c), respectively. The spatial distribution of the upconversion fluorescence of the pump light is plotted in the inset of Fig. 2(a), showing a hexagon pattern. Since the upconversion fluorescence is excited by the pump light, it records the optical intensity distribution of the pump mode, showing that the pump mode possesses hexagon-patterned spatial distribution[30]. And under polygon mode pumping, only the polygon modes other than the WGMs possess enough gain for lasing[30], since the spatial mode overlap between the polygon lasing modes and the polygon pump mode is much higher than that of lasing WGMs. The loaded Q factor Q_L of the pump mode at 974.79 nm was measured as 4.79×10^5 through Lorentz fitting. The coupling efficiency of the pump light was determined as 22.1%. The loaded Q factor Q_L of the lasing mode at 1531.40 nm was measured to 1.28×10^6 through Lorentz fitting. The coupling efficiency of the pump light was determined to be 40.0%. Compared with ultrahigh Q-loaded factors $> 10^7$ in the cold cavity[30], the co-doping of erbium and ytterbium ions will increase absorption loss and degrade the crystal quality, resulting in a reduction of the loaded Q factors. In spite of this, both the polygon pump and lasing modes possess high enough Q factors, resulting from the ultrasmooth surface of the fabricated microdisk and the very weak perturbation.

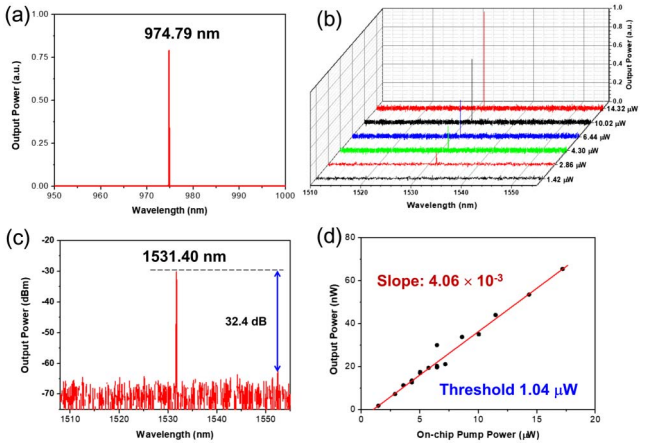

Fig. 3. (a) Spectrum of the pump light at 974.79 nm wavelength; (b) evolution of the output power of the microlaser under different pump power levels; (c) spectrum of lasing signal at 1531.40 nm wavelength, showing a side mode suppression ratio of 32.4 dB; (d) output power dependence on the pump power, exhibiting an ultralow threshold of 1.04 μW and a high conversion efficiency of 4.06×10^{-3}.

4. Demonstration of the Single-Mode Microlaser

A stable single-mode lasing signal was observed at 1531.40 nm when the microdisk was under optical pump at 974.79 nm wavelength with on-chip pump power higher than 1 μW, as shown in Fig. 3. The evolution of the output power of the microlaser under different pump powers is plotted in Fig. 3(b), showing a linear growth. The saturated output power of the microlaser reaches 0.977 μW, corresponding to the side mode suppression ratio of 32.4 dB when the pump power was more than 6 mW. Figure 3(d) plots the output power of the microlaser as a function of the pump power. The output power of the microlaser grows linearly with the increasing pump power, which agrees well with the nature of lasing. The threshold was determined to be ~1.04 μW, which is one order of magnitude lower than the best results reported in single-mode LNOI microlasers[30,42]. A conversion efficiency as high as 4.06×10^{-3} was measured. Both these two values are the best results reported in single-mode active LNOI microlasers, benefiting from the erbium, ytterbium ions co-doping and the excitation of high-Q polygons, which provide high spatial mode overlap between the pump and lasing modes.

5. Conclusion

To conclude, we have demonstrated a stable single-mode microdisk laser in the telecom band with an ultralow threshold based on an erbium-ytterbium co-doped LNOI chip. Thanks to the erbium-ytterbium co-doping providing higher optical gain, the ultralow loss nanostructuring by PLACE, and the excitation

of high-Q polygon modes allowing high spatial mode overlap and suppression of multimode lasing[30,47,49], a threshold as low as 1 μW was achieved. A conversion efficiency up to 4.06×10^{-3} was reported at room temperature. Such a low-threshold single-mode microlaser will promote the development of the scalable photonic integrated circuits on LNOI platforms[50–52].

Acknowledgements

The work was supported by the National Key R&D Program of China (Nos. 2019YFA0705000, 2022YFA1404600, and 2022YFA1205100), the National Natural Science Foundation of China (NSFC) (Nos. 62122079, 12192251, 62235019, 12334014, 12134001, 12104159, and 11933005), the Innovation Program for Quantum Science and Technology (No. 2021ZD0301403), the Shanghai Municipal Science and Technology Major Project (No. 2019SHZDZX01), the Science and Technology Commission of Shanghai Municipality (Nos. 21DZ1101500 and 23ZR1481800), the Youth Innovation Promotion Association of Chinese Academy of Sciences (No. 2020249), and the Engineering Research Center for Nanophotonics & Advanced Instrument, Ministry of Education, East China Normal University (No. 2023nmc005). We thank Dr. Shanming Li and Dr. Yin Hang for providing the erbium, ytterbium co-doped LN crystals and Jingzheng Company for producing the active LNOI wafer.

References

1. C. Wang, M. Zhang, X. Chen, *et al.*, "Integrated lithium niobate electro-optic modulators operating at CMOS-compatible voltages," Nature **562**, 101 (2018).
2. M. He, M. Xu, Y. Ren, *et al.*, "High-performance hybrid silicon and lithium niobate Mach-Zehnder modulators for 100 Gbit s^{-1} and beyond," Nat. Photonics **13**, 359 (2019).
3. R. Wu, L. Gao, Y. Liang, *et al.*, "High-production-rate fabrication of low-loss lithium niobate electro-optic modulators using photolithography assisted chemo-mechanical etching (PLACE)," Micromachines **13**, 237 (2022).
4. A. Rao, K. Abdelsalam, T. Aardema, *et al.*, "Actively-monitored periodic-poling in thin-film lithium niobate photonic waveguides with ultrahigh nonlinear conversion efficiency of 4600 $\%W^{-1}cm^{-2}$," Opt. Express **27**, 25920 (2019).
5. N. Amiune, D. N. Puzyrev, V. V. Pankratov, *et al.*, "Optical-parametric-oscillation-based $\chi^{(2)}$ frequency comb in a lithium niobate microresonator," Opt. Express **29**, 41378 (2021).
6. Y. Zhang, H. Li, T. Ding, *et al.*, "Scalable, fiber-compatible lithium-niobate-on-insulator micro-waveguides for efficient nonlinear photonics," Optica **10**, 688 (2022).
7. J. Lin, N. Yao, Z. Hao, *et al.*, "Broadband quasi-phase-matched harmonic generation in an on-chip monocrystalline lithium niobate microdisk resonator," Phys. Rev. Lett. **122**, 173903 (2019).
8. Y. F. Niu, C. Lin, X. Y. Liu, *et al.*, "Optimizing the efficiency of a periodically poled LNOI waveguide using in situ monitoring of the ferroelectric domains," Appl. Phys. Lett. **116**, 101104 (2020).
9. J. Hou, J. Lin, J. Zhu, *et al.*, "Self-induced transparency in a perfectly absorbing chiral second-harmonic generator," PhotoniX **3**, 22 (2022).
10. L. Wang, X. Zhang, and F. Chen, "Efficient second harmonic generation in a reverse-polarization dual-layer crystalline thin film nanophotonic waveguide," Laser Photonics Rev. **15**, 2100409 (2021).
11. Y.-H. Yang, X.-B. Xu, J.-Q. Wang, *et al.*, "Nonlinear optical radiation of a lithium niobate microcavity," Phys. Rev. Appl. **19**, 034087 (2023).
12. J. Zhao, C. Ma, M. Ruesing, *et al.*, "High quality entangled photon pair generation in periodically poled thin-film lithium niobate waveguides," Phys. Rev. Lett. **124**, 163603 (2020).
13. G.-T. Xue, Y.-F. Niu, X. Y. Liu, *et al.*, "Ultrabright multiplexed energy-time-entangled photon generation from lithium niobate on insulator chip," Phys. Rev. Appl. **15**, 064059 (2021).
14. B.-Y. Xu, L.-K. Chen, J.-T. Lin, *et al.*, "Spectrally multiplexed and bright entangled photon pairs in a lithium niobate microresonator," Sci. China Phys. Mech. Astron. **65**, 294262 (2022).
15. H.-Y. Liu, M. Shang, X. Liu, *et al.*, "Deterministic N-photon state generation using lithium niobate on insulator device," Adv. Photon. Nexus **2**, 016003 (2023).
16. Y. He, Q.-F. Yang, J. W. Ling, *et al.*, "Self-starting bi-chromatic $LiNbO_3$ soliton microcomb," Optica **6**, 1138 (2019).
17. Z. Gong, X. Liu, Y. Xu, *et al.*, "Near-octave lithium niobate soliton microcomb," Optica **7**, 1275 (2020).
18. R. Zhuang, K. Ni, G. Wu, *et al.*, "Electro-optic frequency combs: theory, characteristics, and applications," Laser Photonics Rev. **17**, 2200353 (2023).
19. C. Wang, M. Zhang, M. Yu, *et al.*, "Monolithic lithium niobate photonic circuits for Kerr frequency comb generation and modulation," Nat. Commun. **10**, 978 (2019).
20. C. Yang, S. Yang, F. Du, *et al.*, "1550-nm band soliton microcombs in ytterbium-doped lithium-niobate microrings," Laser Photonics Rev. **17**, 2200510 (2023).
21. S. Wan, P.-Y. Wang, R. Ma, *et al.*, "Photorefraction-assisted self-emergence of dissipative Kerr solitons," arXiv:2305.02590 (2023).
22. B. Fu, R. Gao, N. Yao, *et al.*, "Generation of Kerr soliton microcomb in a normally dispersed lithium niobate microdisk resonator by mode trimming," arXiv:2309.00778 (2023).
23. M. Yu, D. Barton, III, R. Cheng, *et al.*, "Integrated femtosecond pulse generator on thin-film lithium niobate," Nature **612**, 252 (2022).
24. J. Lin, F. Bo, Y. Cheng, *et al.*, "Advances in on-chip photonic devices based on lithium niobate on insulator," Photonics Res. **8**, 1910 (2020).
25. Y. Kong, F. Bo, W. Wang, *et al.*, "Recent progress in lithium niobate: optical damage, defect simulation, and on-chip devices," Adv. Mater. **32**, 1806452 (2020).
26. Y. Jia, L. Wang, and F. Chen, "Ion-cut lithium niobate on insulator technology: recent advances and perspectives," Appl. Phys. Rev. **8**, 011307 (2021).
27. Y. Zheng and X. Chen, "Nonlinear wave mixing in lithium niobate thin film," Adv. Phys. X **6**, 1889402 (2021).
28. J. X. Zhou, R. H. Gao, J. T. Lin, *et al.*, "Electro-optically switchable optical true delay lines of meter-scale lengths fabricated on lithium niobate on insulator using photolithography assisted chemo-mechanical etching," Chin. Phys. Lett. **37**, 084201 (2020).
29. R. Zhang, C. Yang, Z. Hao, *et al.*, "Integrated lithium niobate single-mode lasers by the Vernier effect," Sci. China Phys. Mech. Astron. **64**, 294216 (2021).
30. J. Lin, S. Farajollahi, Z. Fang, *et al.*, "Electro-optic tuning of a single-frequency ultranarrow linewidth microdisk laser," Adv. Photonics **4**, 036001 (2022).
31. Z. Xiao, K. Wu, M. Cai, *et al.*, "Single-frequency integrated laser on erbium-doped lithium niobate on insulator," Opt. Lett. **46**, 4128 (2021).
32. X. Liu, X. Yan, Y. Liu, *et al.*, "Tunable single-mode laser on thin film lithium niobate," Opt. Lett. **46**, 5505 (2021).
33. S. Yu, Z. Fang, Z. Wang, *et al.*, "On-chip single-mode thin-film lithium niobate Fabry–Perot resonator laser based on Sagnac loop reflectors," Opt. Lett. **48**, 2660 (2023).
34. J. Guan, C. Li, R. Gao, *et al.*, "Monolithically integrated narrow-bandwidth disk laser on thin-film lithium niobate," Opt. Laser Technol. **168**, 109908 (2024).
35. J. Zhou, Y. Liang, Z. Liu, *et al.*, "On-chip integrated waveguide amplifiers on erbium-doped thin-film lithium niobate on insulator," Laser Photonics Rev. **15**, 2100030 (2021).
36. Z. Chen, Q. Xu, K. Zhang, *et al.*, "Efficient erbium-doped thin-film lithium niobate waveguide amplifiers," Opt. Lett. **46**, 1161 (2021).
37. Y. Liang, J. Zhou, Z. Liu, *et al.*, "A high-gain cladded waveguide amplifier on erbium doped thin-film lithium niobate fabricated using photolithography assisted chemo-mechanical etching," Nanophotonics **11**, 1033 (2022).

38. S. Wang, L. Yang, R. Cheng, *et al.*, "Incorporation of erbium ions into thin-film lithium niobate integrated photonics," Appl. Phys. Lett. **116**, 151103 (2020).
39. M. Wang, Z. Fang, J. Lin, *et al.*, "Integrated active lithium niobate photonic devices," Jpn. J. Appl. Phys. **62**, SC0801 (2023).
40. Y. Jia, J. Wu, X. Sun, *et al.*, "Integrated photonics based on rare-earth ion-doped thin-film lithium niobate," Laser Photonics Rev. **16**, 2200059 (2022).
41. Y. Chen, "Photonic integration on rare earth ion-doped thin-film lithium niobate," Sci. China Phys. Mech. Astron. **65**, 294231 (2022).
42. Q. Luo, F. Bo, Y. Kong, *et al.*, "Advances in lithium niobate thin-film lasers and amplifiers: a review," Adv. Photonics **5**, 034002 (2023).
43. E. Cantelar, J. A. Muñoz, J. A. Sanz-García, *et al.*, "Yb^{3+} to Er^{3+} energy transfer in $LiNbO_3$," J. Phys. **10**, 8893 (1998).
44. E. Cantelar and F. Cussó, "Competitive up-conversion mechanisms in Er^{3+}/Yb^{3+} co-doped $LiNbO_3$," J. Lumin. **102-103**, 525 (2003).
45. Q. Luo, C. Yang, Z. Hao, *et al.*, "On-chip erbium–ytterbium-co-doped lithium niobate microdisk laser with an ultralow threshold," Opt. Lett. **48**, 3447 (2023).
46. Z. Zhang, S. Li, R. Gao, *et al.*, "Erbium-ytterbium codoped thin-film lithium niobate integrated waveguide amplifier with a 27 dB internal net gain," Opt. Lett. **48**, 4344 (2023).
47. R. Gao, B. Fu, N. Yao, *et al.*, "Electro-optically tunable low phase-noise microwave synthesizer in an active lithium niobate microdisk," Laser Photonics Rev. **17**, 2300903 (2023).
48. R. Wu, J. Zhang, N. Yao, *et al.*, "Lithium niobate micro-disk resonators of quality factors above 10^7," Opt. Lett. **43**, 4116 (2018).
49. B. Fu, R. Gao, J. Lin, *et al.*, "Modes trimming and clustering in a weakly perturbed high-*Q* whispering gallery microresonator," Laser Photonics Rev. **17**, 2300116 (2023).
50. R. Gao, N. Yao, J. Guan, *et al.*, "Lithium niobate microring with ultra-high *Q* factor above 10^8," Chin. Opt. Lett. **20**, 011902 (2022).
51. J. Ma, F. Xie, W. Chen, *et al.*, "Nonlinear lithium niobate metasurfaces for second harmonic generation," Laser Photonics Rev. **15**, 2000521 (2021).
52. Z. He, H. Guan, X. Liang, *et al.*, "Broadband, polarization-sensitive, and self-powered high-performance photodetection of hetero-integrated MoS_2 on lithium niobate," Research **6**, 0119 (2023).